PCCP

PAPER

View Article Online
View Journal | View Issue

Cite this: *Phys. Chem. Chem. Phys.*, 2015, **17**, 3186

Relaxation of a hydrophilic polymer induced by moisture desorption through the glass transition

Xiaolong Zhang,[ab] Hongjiu Hu*[ac] and Manxia Guo[ac]

Received 29th October 2014,
Accepted 11th December 2014

DOI: 10.1039/c4cp04966g

www.rsc.org/pccp

Regarding the underlying special relaxation feature of a water-plasticized hydrophilic polymer during performance evolution with water content change, we report the water desorption kinetics and periodic creep responses of poly(vinyl alcohol) (PVA) films subsequent to rejuvenation by above-glass transition relative humidity (RH) annealing and following RH-jump at various rates. A Moisture Sorption Analyzer and a Dynamic Mechanical Analyzer are utilized to control RH and to capture data to probe the evolving relaxation towards equilibrium under two temperature–RH conditions. This result reveals an evident jump rate dependence of desorption kinetics and recoverable creep deformation. The different target RH yields the different change patterns of normalized water content and retardation time. PVA manifests a rapid relaxation stage with the special viscoelastic response before experience of usual physical aging. By analysis of the superposition principle and the relevant characteristic parameters, the relaxation of the hydrophilic polymer after water desorption through the glass transition is generalized as three successive phases.

1. Introduction

It is usually referred to as the plasticization effect when a glassy polymer is brought into contact with moisture and thereby absorbs water molecules. This signature results in decrease of glass transition temperature and degradation of stiffness and strength, which are primarily governed by the change in plasticizer concentration.[1,2] Analogous to glass transition induced by temperature change, external relative humidity variation and the resulting change in water content can also lead to a marked viscoelastic state change of the glassy polymer with corresponding critical conditions denoted by the glass transition relative humidity (RH_g)[3,4] or the critical relative humidity (RH_c).[5]

Another unique feature of the glassy polymer relates to its nonequilibrium thermodynamic state, which typically originates from cooling below the glass transition temperature (T_g). The spontaneous evolution of the molecular structure towards equilibrium at a fixed temperature is generally known as structural relaxation and the associated effects on physical and mechanical properties are usually called "physical aging".[6] The obvious consequences of physical aging with constant consolidation of structures are the change in macroscopic properties, *e.g.* mass density, stiffness, enthalpy, permeability, the dielectric constant, the refraction index and also absorption capacity.[7–13]

Studies regarding temperature-dependent properties of a glassy polymer, particularly for the relaxation in relation to physical aging, have been extensively reported, and many excellent reviews were written.[14–18] However, when taking into account moisture factors, especially for the relaxation of the aforementioned glassy polymer formed by water content change, the existence of water and its concentration variation enable the material to behave in a more complex manner that differs from usual aging, which still remains to be thoroughly characterized. Meanwhile, as large water content variation substantially relates to the conformation change of polymer molecular structure in a microscopic view,[19–21] the coupled concentration gradient-dependent diffusion and time-dependent molecular relaxation driven by multiple thermodynamic forces highlight the need for more comprehensive consideration. This is clearly a concern for applications of hydrophilic polymers simply because of their strong sensitivity to humidity as well as their ubiquitous humid surroundings arranged to achieve specific functions or encountered inevitably during processing and storage.

The similar effects of temperature and relative humidity on mechanical performance have caused researchers to focus on the impact of humidity on glassy stability[22–25] and durability regarding hydrothermal degradation.[26–28] However, for various reasons, only a few studies in the literature exist on analysis of viscoelastic response and the relaxation mechanism of a glassy polymer in a mechanical way considering moisture factors, especially RH variation. The pioneering investigations were

[a] *Shanghai Institute of Applied Mathematics and Mechanics, Shanghai University, Shanghai 200072, China. E-mail: huhongjiu@shu.edu.cn; Tel: +86 021 56338345*
[b] *Department of Aerospace Engineering and Applied Mechanics, Tongji University, Shanghai 200092, China*
[c] *Shanghai Key Laboratory of Mechanics in Energy Engineering, Shanghai 200072, China*

made by McKenna and co-workers.[4,29,30] In their experiments, epoxy films were subjected to rapid changes in surrounding RH and the resulting volume recovery and physical aging response were tracked.[4,29] The qualitative similarity but quantitative differences between RH-jump responses and temperature-jump responses were systematically analyzed.[30] It is also important to find that the above-RH_g treatment is beneficial to increase the glassy-state stability of epoxy. Epoxy resin, however, primarily as a structural material, has relatively low water uptake in comparison to hydrophilic polymers. The very limited active contribution of water results in comparatively fewer responses in a typical observation time scale for aging.

Another focus of attention usually falls on the reversibility of physical aging by increasing material free volume. Thermal rejuvenation is the currently most effective approach, where annealing above T_g for adequate time is a conventional (but not a necessary) way.[31–34] Compared with substantial studies in the literature that have been addressing this issue for various materials, few studies have discussed the sub-T_g rejuvenation of a hydrophilic polymer *via* moisture adjustment as well as the new-generated relaxation process. In addition, no previous investigation has identified the effect of RH-jump rate on the relaxation behavior. Thereupon, the practical effectiveness of above-RH_g annealing for de-aging should be further evaluated, and the subsequent desorption induced relaxation in the glassy state deserves detailed investigation.

In this study, we concentrate on the effect of RH change on relaxation behavior of a hydrophilic polymer in the light of prevalent impact of moisture in practice. Specifically, as a representative hydrophilic polymer, poly(vinyl alcohol) (PVA) is used as experimental material to investigate the evolving relaxation behavior after a series of isothermal sorption–desorption by capitalizing on the ability of the Dynamic Mechanical Analyzer equipped with a RH-Accessory. To ensure the reproducibility of experiments, reliability of rejuvenation *via* RH annealing is verified firstly. Realizing that the influence of RH is substantially embodied in water sorption and desorption with changing sample weights, water desorption experiments are next carried out to capture the desorption kinetics that assist in comprehending desorption induced properties. To study the RH-jump rate dependence of glass transition and RH dependence of the relaxation pattern, various rates as well as different target RH are emphasized in the periodic creep experiments. The time–aging time superposition and time–RH-aging time superposition are subsequently discussed. Finally, but most importantly, the variations of characteristic parameters of viscoelasticity are analyzed in detail to elicit the interpretation of the multi-stage relaxation process.

2. Experimental

2.1. Materials

PVA films were prepared using the following procedure. Poval® PVA-224 (Kuraray, Osaka, Japan) powder with an alcoholysis degree of 87–89% was dissolved in distilled water at 95 °C for 3 hours under stirring at 90 r min^{-1}, which resulted in PVA aqueous solutions (10 wt%). After the solutions were slowly cooled to room temperature (25 °C), they were casted onto leveled Teflon coated glass plates, and desiccated in a vacuum oven at 35 °C for 2 days. Dried samples were annealed at 120 °C for 30 min to erase prior thermal history, and then they were cut to dimensions 40 mm × 5 mm × 0.03 mm (5 mm × 5 mm × 0.03 mm for desorption tests) and kept in the dry state at room temperature. As can be seen in Fig. 1(a), the testing film specimens show a flat and smooth surface with no bubbles, which may indicate the uniform distribution of PVA molecules throughout the films. A thickness of 0.03 mm was selected to facilitate efficient water transfer throughout the film, and thereby making it possible for faster water content equilibrium. The practical equilibration time for sorption/desorption kinetics is approximately 30 min at 30 °C, 30–80% RH determined by a Moisture Sorption Analyzer (see Fig. 1(b)). The T_g of the dry sample is 85.5 °C as measured by DMA (tan δ, 1 Hz).

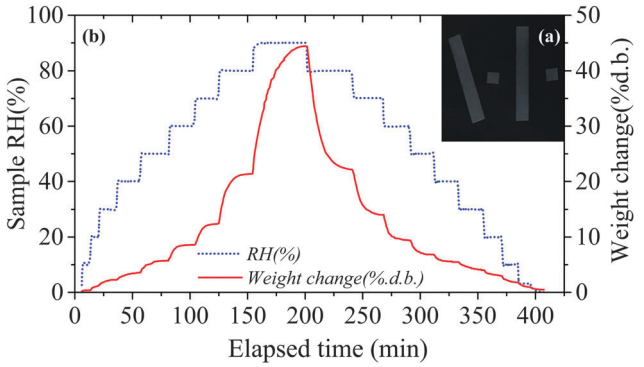

Fig. 1 (a) PVA film specimens and (b) kinetic curves of PVA at 30 °C measured by a Hiden® IGAsorp Moisture Sorption Analyzer at 200 sccm.

2.2. Water desorption kinetics

A Hiden® IGAsorp Moisture Sorption Analyzer was applied to capture the water desorption kinetics of PVA films after a rapid decline of external RH. The IGAsorp instrument can regulate the sample chamber RH within 0–95% by mixing different percentages of N_2–H_2O gas. The accuracy of the RH sensor is ±1% (0–90% RH), ±2% (90–100% RH) and the linear RH ramping rate is 0.1–120% per hour. The sample chamber temperature is controlled by a water bath within 5–80 °C (±0.05–0.1 °C). The maximum weighing capacity is 200 mg with resolution of 0.1 μg/100 mg.[35] The method for water desorption measurement is as follow: PVA films (30–40 mg) were loaded in the balance of IGAsorp and the temperature was initialized at 30 °C. Films were then dried at 120 °C, 0% RH, for 2 hours, and equilibrated at 30 °C, 90% RH (200 sccm), for 2 hours to ensure sufficient moisture sorption. Subsequently, the RH levels were adjusted isothermally to 30% and 40% with rates of 1% min^{-1}, 1.5% min^{-1} and 2% min^{-1}, respectively. Once the target RH was stable, water content was measured for more than 2000 min.

2.3. Creep measurements

Uniaxial tension creep responses of PVA films were measured using TA Instruments DMA Q800. By utilizing the DMA

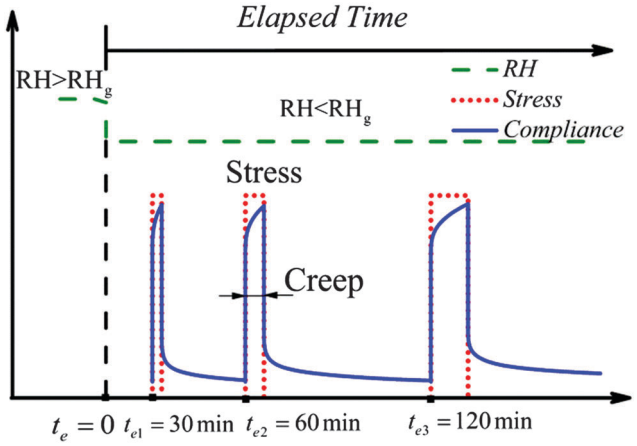

Fig. 2 Short-term creep measurements performed with Struik's protocol.

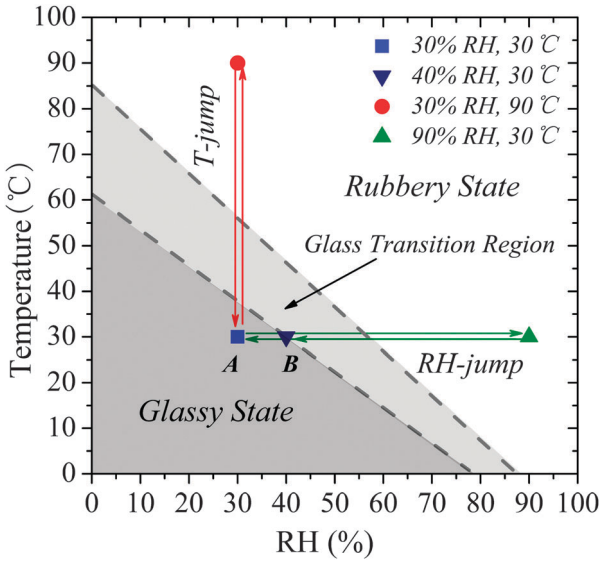

Fig. 3 State diagram of PVA with RH–temperature paths in rejuvenation and RH-jump experiments.

RH-Accessory, RH regulation of the sample chamber was realized by controlling pure N_2 and a saturated water vapour mixture of different proportions. The maximum humidity ramp rate is 2% min^{-1}, both linear increasing and decreasing with time, meanwhile, the sample temperature can be kept within ±0.5 °C over the range 5–120 °C. More specifications for the RH-Accessory were expanded elsewhere.[3,36] To investigate the relaxation process, following the line of thought originally suggested by Struik,[6] the classical design of the physical aging experiment as depicted in Fig. 2 was used to implement the periodic short-term creep measurements. In detail, the samples were subjected to a sequence of creep with 2 MPa applied stress and succeeding recovery after each RH adjustment. During this period, the creep compliances were monitored. To neglect the influence of individual creep tests on the sample properties, each creep duration was short in comparison with the previous elapsed time as well as the later recovery period. This requires that creep time is equivalent to or less than 10% total elapse time.[6,14] The first creep-recovery cycle started at 30 min after the end of the RH-jump (zero time); the initial time of the next cycle was twice that of the previous, and the like.

2.4. Relaxation process study

The study on relaxation behavior was performed at a fixed temperature. As illustrated in the state diagram (Fig. 3), two experiments were formulated: rejuvenation and RH-jump.

2.4.1 Rejuvenation experiment. The rejuvenation experiment was set to verify the reliability of sub-T_g annealing at high RH upon elimination of thermal history. The PVA samples were firstly held at 30% RH, 90 °C (> T_g at 30% RH) for 30 min to erase thermal history, and then the temperature was reduced to 30 °C at 1 °C min^{-1} to perform the creep tests. After some aging time, the RH was raised to 90% (> RH$_g$ at 30 °C) and maintained for 2 hours isothermally, and then it was reduced to 30% at 1% min^{-1} to carry out the second creep tests.

2.4.2 RH-jump experiment. After the samples were annealed at 90% RH (> RH$_g$ at 30 °C), 30 °C for 2 h, the RH was adjusted to target levels at rate of 0.1% min^{-1}, 1% min^{-1}, 1.5% min^{-1} and 2% min^{-1}, respectively. The creep compliances were measured at different elapsed times. According to the state diagram (Fig. 3), two target RHs were concerned: 30% (condition A) and 40% (condition B), which represent two typical states of glassy PVA: the deep glassy state and near the glass transition.[3,16]

3. Theoretical basis

The Kohlrausch[37]–Williams–Watts[38] (KWW) function $J(t) = J_0 e^{(t/\tau)^\beta}$ is used to characterize the basic feature of creep curves, where J_0 is the initial creep compliance, t is the creep time, τ is the characteristic retardation time which depends on specific conditions under consideration, and β is the shape factor associated with viscoelasticity. It should be mentioned that the modified KWW equation $J(t) = J_0 + J_1(1 - e^{-(t/\tau)^\beta})$ and other similar functions are not applied here because the KWW function yields the best-fitting results when exercised to our data in all cases.

Creep curves with different retardation time τ can be shifted to form a master curve following the relation $J(t,\tau^{ref}) = J(t/a(t),\tau)$ providing β is a constant, where τ^{ref} is retardation time at the reference state and $a(t)$ is the horizontal shift factor. The temperature and RH dependence of creep compliance is embodied in the time–temperature superposition principle[1,39] and the time–RH superposition principle,[40,41] namely we have

$$J(T_{ref}, RH_{ref}, t) = J(T, RH, t/\phi) \quad (1)$$

where, $\phi = a_T \cdot a_{RH}$ is the hydrothermal shift factor and a_T, a_{RH} are the temperature shift factor and RH shift factor, respectively.

In terms of a usual physical aging process, the time-aging superposition works. The creep curves of quenched polymers are nearly horizontally shifted towards longer times with increasing aging time.[6,15,42] The horizontal shift factor

$$a(t_e) = \tau(t_e)/\tau(t_e^{ref}) \quad (2)$$

is used to represent the shift interval between compliance curves at the reference aging time t_e^{ref} and aging time t_e.[6]

Sometimes additional vertical shift $b(t_e) = J_0(t_e)/J_0(t_e^{ref})$ is also necessary.[6,29] The calculated $a(t_e)$ and $b(t_e)$ are used to generate the master curve; however a manual shifting method is also an effective way,[29] by which one superimposes the compliance curves to the reference curve along the time axis manually. The shift rate μ defined by

$$\mu = \frac{\mathrm{d}\log a(t_e)}{\mathrm{d}\log t_e} \quad (3)$$

is obtained from a double logarithmic plot of $a(t_e) - t_e$ and it may be a function of aging time[42,43] or other variables.[44,45]

It should be noted that the expression ''elapsed time'' instead of ''aging time'' will be used in what follows considering the preciseness. Nevertheless, we still keep using some terminologies of physical aging like ''time-aging superposition'' for convenience.

4. Results

4.1. Rejuvenation after annealing above RH_g

To characterize the responses of PVA samples after RH-jump from the above-RH_g condition, one should begin with the fundamental basis of verifying the reliability of rejuvenation *via* humidity change, although the above-RH_g exposure is found to cause glassy–rubbery transition[3–5,28,46] and thus affect the thermal history. Following the previous design, two sets of samples' creep responses (the one aging at 30 °C, 30% RH after thermal quench from 90 °C, 30% RH at 1 °C min^{-1}, and the other evolving under the same condition after a sequential RH-jump from 30 °C, 90% RH at 1% min^{-1}) are compared. It is found that, at the same elapsed time, creep compliances of the two sets increase with creep time gradually, but their magnitudes vary. That is, at the same creep time, the creep compliance appears to be much larger after RH annealing compared with that during aging after the previous thermal quench. Meanwhile, the retardation time τ of PVA by moisture treatment obviously decreases. For the first creep-recovery cycle, we have J_0 = 936.2 ($\mu m^2\ N^{-1}$), τ = 17.4 (s) and J_0 = 283.5 ($\mu m^2\ N^{-1}$), τ = 5172.6 (s) for the RH annealed set and the thermal aging set, respectively. These rejuvenated creep responses imply that the RH-jump from the above-RH_g condition endows the new-formed glassy polymer a relatively high molecular mobility to drive the polymer far from the equilibrium state, and thus be effective to wipe off the thermal history.

4.2. Water desorption kinetics

The intrinsic isotherm denoted by Kovacs' classic kinetic experiment of temperature-jump[39] reveals the continuous evolution of excess volume of the glassy polymer. The isotherm presents larger volume departure and longer equilibrium time at lower target temperature below T_g. Similar experiments considering humidity change were carried out by Zheng and McKenna,[4] where a series of RH-jump tests were designed and the resultant isopiestics show larger volume departure and also longer equilibrium time at lower RH below the sample RH_g. The volume recovery after cooling process develops without sample mass change. The moisture effect is substantially determined, however, by water mass transfer during sorption and desorption. Desorption kinetics analogous to intrinsic isopiestics is thus to be best with capturing the desorption-related response after RH-jump to some extent. When a polymer in equilibrium under above-RH_g conditions undergoes a rapid RH decline, the decreasing water content may lag behind the corresponding external RH, *i.e.* deviate from the equilibrium water content.[47–49] Once the polymer passes through the rubbery to glassy transition with decreasing RH and finally reaches the target sub-RH_g condition, the hysteresis makes the excess water content evolve as a function of elapsed time.

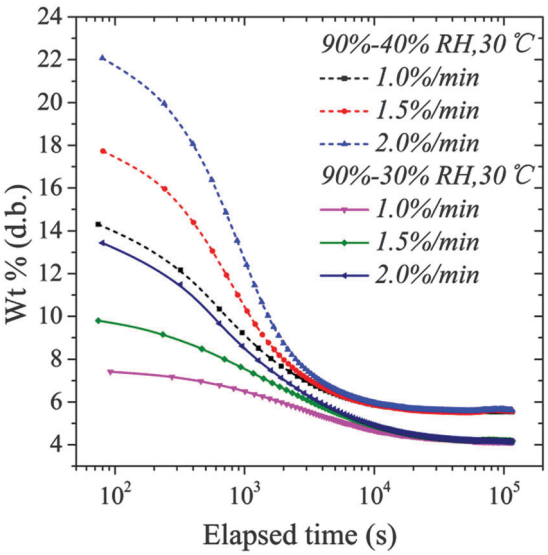

Fig. 4 Desorption kinetic curves of PVA films at 40% RH, 30 °C and 30% RH, 30 °C after RH-jump from 30 °C, 90% RH at different rates.

Accordingly, the PVA films with relatively high water content are in a rubbery state after they absorbed enough water at 30 °C, 90% RH. The succeeding rapid RH adjustment to sub-RH_g values 30% RH and 40% RH at different rates results in moisture induced glass transition and excess water content. As depicted in Fig. 4, the water contents of PVA films under all conditions are observed to decrease with time at a decreasing rate until the approach to the equilibrium. The higher target RH leads to larger water content at any time, and the higher jump rate also yields greater water content at the initial stage. However, this rate dependence becomes less obvious as the time increase.

Analogous to the volume departure,[4,14,39] it is reasonable to define the normalized water content to epitomize the water content departure from equilibrium:

$$\delta_{wt}(t) = \frac{\mathrm{Wt}(t) - \mathrm{Wt}_\infty}{\mathrm{Wt}_\infty} \quad (4)$$

where, Wt(t) and Wt_∞ are water content at time t and equilibrium state, respectively. The evolvement of δ_{wt} is graphed in Fig. 5. Under each RH condition, the rate dependence is similar to that in kinetics curves (Fig. 4). During the initial stage, the higher RH value leads to larger water content, but a shorter time to approach to the equilibrium simultaneously (Fig. 5(a)).

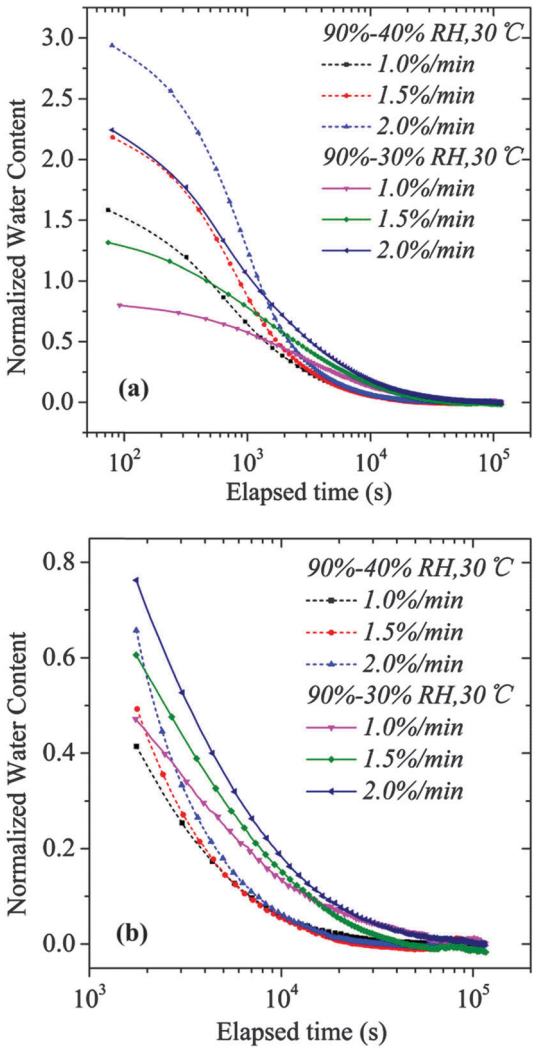

Fig. 5 The normalized water content of PVA films as a function of elapsed time at 40% RH, 30 °C and 30% RH, 30 °C after RH-jump from 90% RH, 30 °C at different rates: (a) time from 0 min to about 2000 min and (b) time from 30 min to about 2000 min.

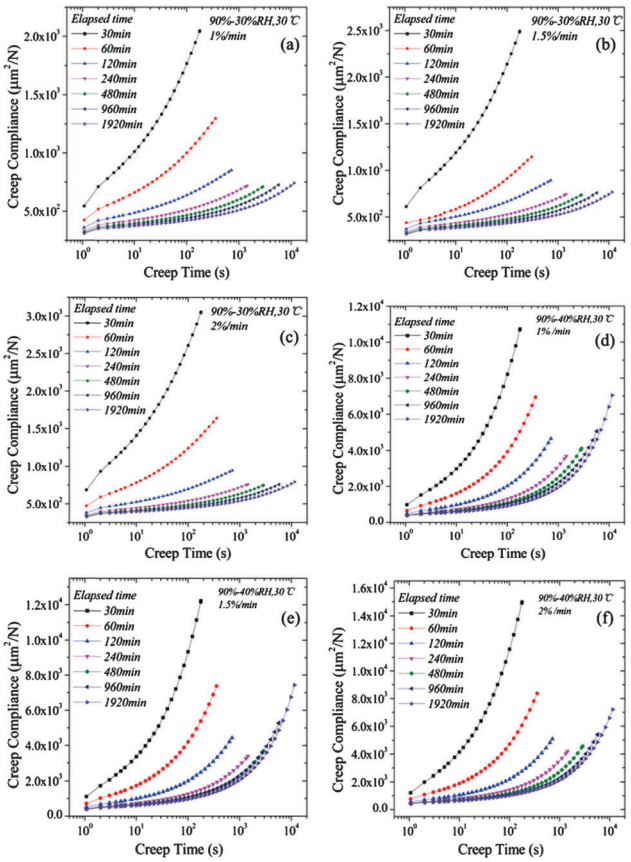

Fig. 6 Creep responses of PVA films after 2 h annealing at 90% RH, 30 °C and RH-jump at different rates to 30% RH, 30 °C: (a) q = 1.0% min^{-1}, (b) q = 1.5% min^{-1}, (c) q = 2.0% min^{-1} and to 40% RH, 30 °C: (d) q = 1.0% min^{-1}, (e) q = 1.5% min^{-1}, (f) q = 2.0% min^{-1}.

However, for time longer than 30 min, the rapid decrease of water content at 40% RH makes the curve of δ_{wt} gradually below that of 30% RH (Fig. 5(b)). The δ_{wt} curves at 30% RH are also found to decrease evidently at the later period compared with curves at 40% RH with almost unchanged slope. It is important to notice that these variations may imply the different movement patterns of water molecules and polymer structures as well as the characteristic time gap of the movement between the earlier and later period of evolution under two RH conditions.

4.3. Creep responses

Fig. 6 plots the short-term creep responses of PVA samples at 30% RH, 30 °C and 40% RH, 30 °C during relaxation after the RH-jumps at rates 1% min^{-1}, 1.5% min^{-1} and 2% min^{-1}, respectively. A sequence of loading time from 30 min to 1920 min is considered. It can be concluded from these figures that the creep compliances increase with creep time in an increasing rate, and decrease with elapsed time in a decreasing rate under all conditions. These change patterns illustrate the decreasing molecular mobility and thus recovery rate drops of molecular structure during relaxation.

It is necessary to figure out the regularity of compliance evolution. Accordingly, the characteristic parameters (initial creep compliance J_0 and retardation time τ), derived from these creep compliances by KWW model, are given in Fig. 7 and 8.

4.3.1 Initial creep compliance. As shown in Fig. 7 (0.1% min^{-1} case excluded), under any RH condition, the initial creep compliances J_0 of PVA samples decrease with increasing elapsed time in a considerable deceasing rate after RH-jump. Particularly, the rapid decline of sample flexibility denoted by the sharp drop of compliances at the initial stage indicates significant relaxation in molecular structure due to the evident total mass loss and volume shrinkage induced by water desorption. However, the variation of J_0 next turns to be less intense which behaves like a physical aging process with a moderate rate. The J_0 curves at 40% RH are all above those at 30% RH at any time, owing to the higher flexibility of the local molecular segment contributed by more imbibed water. The jump rates separate the curves, and the higher rate yields the larger J_0 value especially at the initial stage, which is consistent with the greater water content kept in PVA at a high RH-jump rate (see Fig. 4).

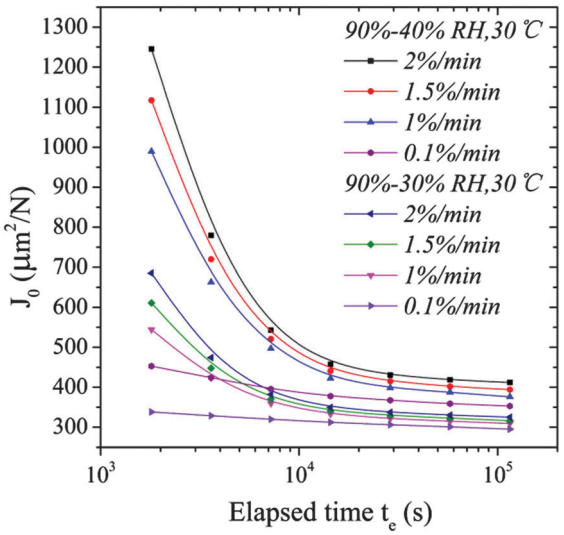

Fig. 7 Initial creep compliance J_0 of PVA films at 30% RH, 30 °C and 40% RH, 30 °C after RH-jump at different rates.

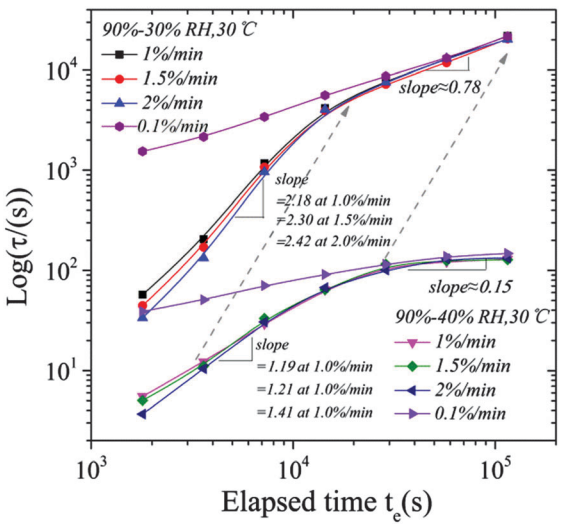

Fig. 8 Retardation time τ of PVA films *versus* elapsed time at 30% RH, 30 °C and 40% RH, 30 °C at different RH-jump rates.

4.3.2 Retardation time. The bi-logarithmic diagram of retardation time τ *versus* elapsed time of PVA films (Fig. 8) presents a more graphic description of the relaxation process. The retardation time increases dramatically with increasing elapsed time in all cases and an obvious turn occurs in the middle (0.1% min^{-1} case excluded). The curves appear to be a near-bilinear pattern with two characteristic slopes, and a smooth transition within them. Due to the stronger motion ability of molecules and thereby shorter time to respond to external load at higher RH, retardation times at 40% RH are far smaller than those at 30% RH at the same elapsed time and the differences become more evident as increasing time. As a result of the higher water content departure, the influence of the RH-jump rate appears more markedly at the initial stage where the rate of 2.0% min^{-1} yields the minimum retardation time.

5. Discussions

5.1. Time–aging time superposition

Considering the time–aging time superposition of a usual physical aging process, aging shift factor determined by eqn (2) is generally a preference to build the master curve. However, as for the RH-jump procedure, the applicability of the formula needs to be checked. The creep data at 30 °C, 30% RH following RH-jump at 1.5% min^{-1} is selected as an instance, where t_e = 1920 min is set as the reference state and the rest of curves are shifted to it with a horizontal interval calculated by eqn (2).

As shown in Fig. 9, the horizontal shift alone is obviously inadequate to form the desired master curve for data at the initial stage, and the additional vertical shift cannot contribute to a better result either. The main reason accounting for this is the insufficiently calculated horizontal shift interval. Due to the large excess water content and its continued evolution throughout the creep tests at the initial stage, there appears to be a different relaxation pattern compared with the later period which can be interpreted as physical aging where superposition using eqn (2) is still available.

To proceed with analysis on such a feature, the alternative way lies on manual shift. The PVA master curves are generated

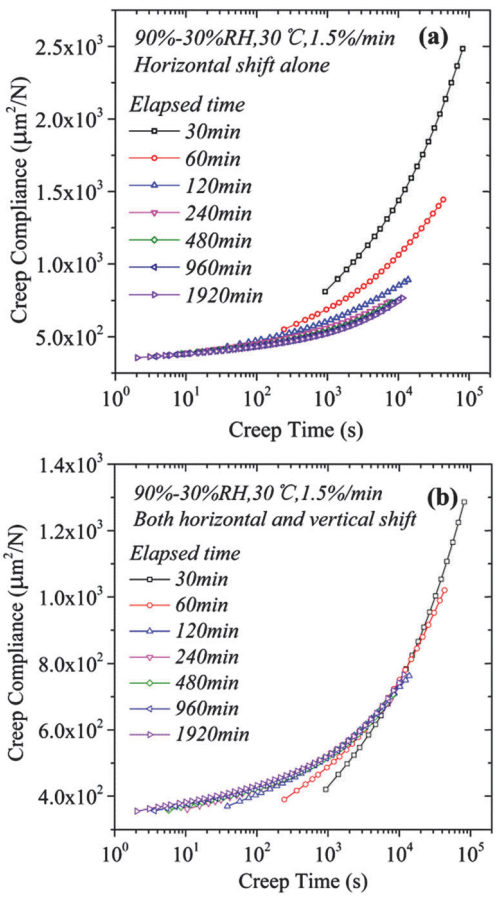

Fig. 9 Master curve building using the shift factor in eqn (2) of PVA: (a) horizontal shifts alone and (b) both horizontal shifts and vertical shifts.

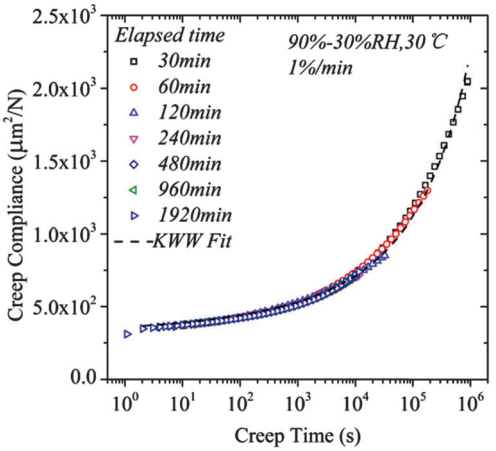

Fig. 10 Master curve of PVA creep data at 90–30% RH, 30 °C, 1% min^{-1} by manual shifts and the related KWW fitting.

manually by setting the creep curves at t_e = 1920 min as the reference state. We can find that the superposition of master curves by horizontal shifts alone exhibits the high quality in all cases. For brevity's sake, only part of the result (30% RH, 1% min^{-1}) is plotted in Fig. 10. The excellent correlations are also found in related KWW-fitted curves ($R^2 > 0.987$). The validity of manual shifts implies the unchanged shape of creep curves, though we have inferred the existence of underlying distinction in the relaxation pattern in the initial stage and the later period.

The manual shift factors $a(t_e)_m$ as a function of elapsed time are shown in Fig. 11. Shift factors $-\log a(t_e)_m$ decrease with increasing elapsed time under all conditions. Similar to the retardation time (Fig. 8), these curves exhibit a bilinear trend with smooth transitions in the middle (0.1% min^{-1} case excluded). The absolute values of slopes of $\log a(t_e)_m - \log t_e$ plots, in fact, define the shift rate μ in a similar way compared to $\log \tau(t_e) - \log t_e$ plots. The difference, which may vanish in the usual physical aging process after thermal quenching, arises from the above fact that the actual shift rate cannot be deduced from $\log \tau(t_e) - \log t_e$ plots using shift factor with eqn (2) in the earlier period after RH-jump.

5.2. Time–RH-aging time superposition

The RH dependence of relaxation is reconsidered in referring to time–RH-aging time superposition. The total shift factor is given by $\phi = a_{te} \cdot a_{RH}$ based on the eqn (1). The principle is applied to an instance of creep data at different RH with an identical jump rate. Specifically, the creep curve at 40% RH, 480 min is shifted to the curve at 30% RH, 1920 min manually (time–RH-aging time superposition). Meanwhile, the creep curve at 40% RH, 1920 min is shifted to the curve at 30% RH, 1920 min (time–RH superposition). The corresponding results shown in Fig. 12 demonstrate the good agreement of the reference curve and shifted curves.

5.3. Multi-stage relaxation

To discuss the entire relaxation process, the shift rates, *i.e.* the absolute values of the linear slope of two sets of $\log a(t_e) - \log(t_e)$ curves, were compared and evident target RH dependence is found. The $\log a(t_e) - \log(t_e)$ curves (see Fig. 11, 0.1% min^{-1} case excluded) at 30% RH are approximately composed of two straight lines with a slope above 3.0 and around 0.82 connected by a characteristic transition; the curves at 40% RH comprise of lines with a slope above 2.0 and 0.18. Likewise, the $\log \tau(t_e) - \log t_e$ curves at 30% RH (0.1% min^{-1} case excluded) correspond to lines with a slope above 2.0 and about 0.79, and the curves at 40% RH correspond to lines with slope around 1.0 and 0.15 (see Fig. 8). These similar curve shapes but different slopes imply the inherent difference of the relaxation pattern. Regarding the physical aging after thermal quenching, the higher aging temperature accelerates the aging to actualize

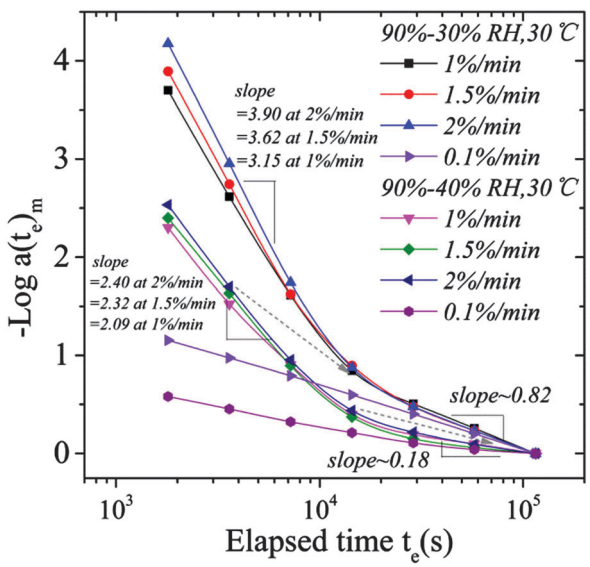

Fig. 11 The bi-logarithmic plots of the manual shift factors *versus* elapsed time of PVA films.

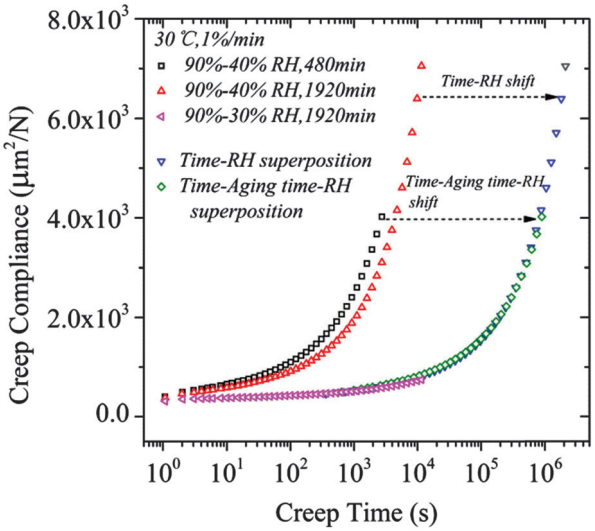

Fig. 12 Verification of the time–RH-aging time superposition of PVA creep curves.

the observation of aging equilibrium in the laboratory time scale.[6,14] In this case, the polymer manifests a bilinear behavior in the $\log a(t_e) - \log(t_e)$ plot with typical slopes at around 1.0 and 0.1 representing aging and equilibrium stages respectively, and the inflection point is denoted as equilibrium time t_e*.[14,15,42,50] Analogously, we distinguish the underlying pattern of two sets of $\log a(t_e) - \log(t_e)$ or $\log \tau(t_e) - \log t_e$ curves by comparing the shift rate. As a result, the evolution at 40% RH (near the glass transition) is considered to be the relaxation associated with aging and the subsequent aging equilibrium. This interpretation can be evidenced by corresponding desorption data. For the elapsed time more than 3×10^3 (s), water desorption has almost completed. The nearly unchanged water content corresponds to the relatively moderate increasing of $\log \tau(t_e)$ that is predominated by structural recovery. However, the case at 30% RH (deep in glassy state) is very different. In view of the shift rate analysis and continuous decrease of δ_{wt} at the later period of desorption, it is rational to infer that the evolution at 30% RH (0.1% min^{-1} case excluded) corresponds to a smooth connection of the former relaxation with rapid volume shrinkage predominated by water desorption and the following aging process dominated by a spontaneous conformation rearrangement. Actually, it is easy to observe that the elapsed time corresponding to the transition in bilinear log $a(t_e)$ and $\log \tau(t_e)$ at 30% RH is approximately equal to the time that desorption nearly completes, which directly reveals the impact of the difference in the dominant factor of relaxation before and after the transition on the viscoelastic response. The second turn in $\log a(t_e) - \log(t_e)$ or $\log \tau(t_e) - \log t_e$ curves at 30% RH that means aging equilibrium could be reasonably expected if the experiment continues.

From this perspective, the relaxation process of a hydrophilic polymer after RH-jump through RH_g, or generally the water desorption through the glass transition at the fixed temperature may be generalized as three phases: (a) rapid relaxation in the molecular structure predominated by water desorption. In this phase, the relatively high molecular mobility induced by excess water brings very small relaxation time, and the rearrangement of polymer structure is immediately driven by the migrating water. With the continuous shrinkage of available space for molecular motion, the self-deceleration thermodynamic property gradually takes effect to retard the further conformational change that once coordinates with the water loss. Realizing the coexistence of spontaneous recovery in molecular structure, perhaps it is difficult to decouple the consolidation driven by configurational entropy from the practical process; (b) relaxation associated with physical aging. The increasing gap between retarded molecular motion and evacuation of residual water results in vacancy once occupied by water. Thereafter, the relaxation associated with aging begins to manifest itself with dissipation of the residual excess volume; (c) physical aging equilibrium (monitored mechanically). Considering the strong history effect of viscoelastic material, the existence of previous desorption dominated period is likely to account for the intrinsic difference in physical aging rate between materials after RH-jump and cooling[29,30] and even between polymers with different hydrophilicity.

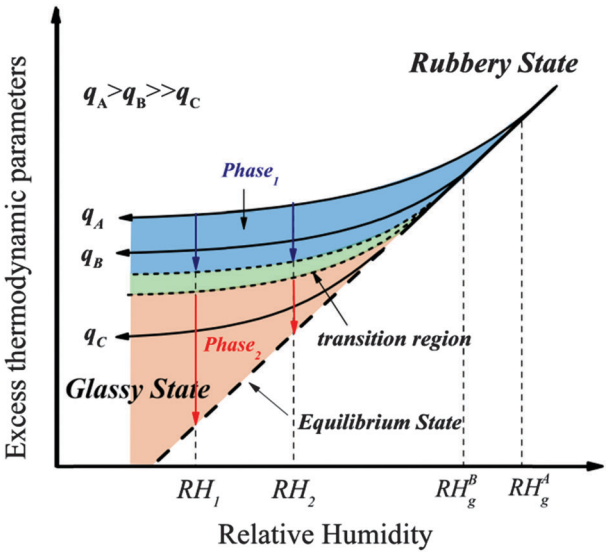

Fig. 13 Illustration on the rate dependence of the relaxation process of a hydrophilic polymer after RH-jump through RH_g.

To give a brief illustration on the above speculations, we consider the classic schematic of glass formation (Fig. 13). A humidity process is present here instead of the temperature one where RH-jump from a high RH to sub-RH_g condition yields a departure from equilibrium whose extent highly depends on the jump rate and target RH. According to our data, the relaxation towards the equilibrium which refers to physical aging after a cooling process is replaced here by a multi-stage process with a transition region that divides the area below the jump curve into two parts. The results at 40% RH demonstrate that relaxation at higher RH (RH_1 in Fig. 13) yields larger proportion of the desorption dominated phase, and thus produces aging dominant results for a relatively late observation.

As an indirect evidence of multi-stage relaxation, the RH-jump rate dependence is reconsidered by setting of an extreme case with very low rate at 0.1% min^{-1}. Low jump rate brings low RH_g,[5] small excess thermodynamic variables and low water content as well. According to Fig. 13, the low rate should bring an aging process without evident desorption-dominated relaxation due to it mainly occurs during the jump procedure before reaching the target RH. The corresponding example illustration is presented in Fig. 7, 8 and 11. The moderate declines of creep compliance as well as near-linear $\log \tau(t_e)$ and $\log a(t_e)$ without apparent transition demonstrate their significant difference from the others; that is, the physical aging nature in the whole time window. RH-jump at 0.1% min^{-1} also exhibits the lowest shift rate in all cases as denoted by Fig. 8 and 11.

In the calculation of the characteristic parameter for long term response predictions, one must account for the change in the shift rate caused by the twice transition of the relaxation process. As a generalization, a trilinear form shift factor corresponds to the multi-stage relaxation is plotted in the diagrammatic sketch (Fig. 14). We denote that the characteristic time at

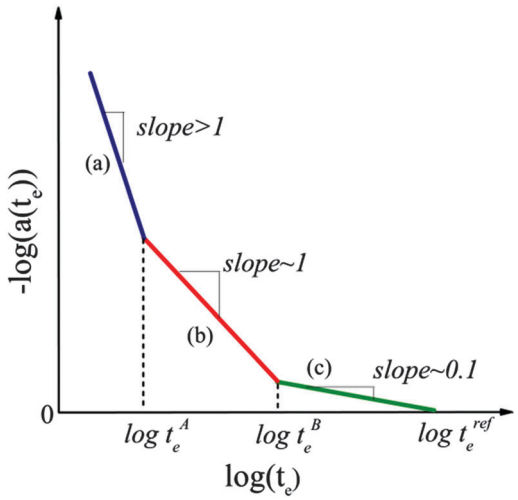

Fig. 14 A generalized trilinear form shift factor of a hydrophilic polymer after desorption through the glass transition.

the inflection point as t_e^A and t_e^B, respectively, denote the characteristic shift factors as $a_{t_e^A}$, $a_{t_e^B}$ and $a_{t_e^{ref}}$. Expressing the shift rates in different phases as the corresponding slopes and noting the identity $\log a_{t_e^{ref}} = 0$, one can find

$$a_{t_e} = \left(\frac{t_e}{t_e^A}\right)^{\mu_1}\left(\frac{t_e^A}{t_e^B}\right)^{\mu_2}\left(\frac{t_e^B}{t_e^{ref}}\right)^{\mu_3} \quad (5)$$

for any $t_e < t_e^A$. It would reduce to $a_{t_e} = (t_e/t_e^*)^{\mu_1}\cdot(t_e^*/t_e^{ref})^{\mu_2}$ in a bilinear case, where t_e^* is the aging equilibrium time observed by creep experiments. By combining eqn (5) and (2), the retardation time at any elapsed time can be calculated.

6. Conclusions

We have presented the investigation on desorption kinetics, creep responses of PVA films subsequent to a series of water sorption and desorption processes at a fixed temperature using a Moisture Sorption Analyzer and a Dynamic Mechanical Analyzer. Effects of RH-jump rates and RH conditions were investigated. We found that, PVA, a typical hydrophilic polymer, shows a multi-stage relaxation process after RH-jump from above-RH_g to sub-RH_g conditions, including the rapid relaxation predominated by water desorption, relaxation associated with physical aging and aging equilibrium. The change of creep behaviors and desorption kinetics demonstrate the influence of a different relaxation mechanism on the macroscopic physical properties. Importantly, the manual shift method can be used to build the master curve of the hydrophilic polymer during the whole relaxation process. Compared with bilinear logarithmic retardation time at 1–2% min^{-1} jump rate, the near linearity feature of logarithmic retardation time at a very low RH-jump rate (0.1% min^{-1}) reveals the strong jump rate dependence of the relaxation pattern of the hydrophilic polymer observed at a fixed observation time window. We hope the above discussions could lead to a better understanding of RH-related properties of polymers as well as fuel more critical assessment in terms of desorption induced relaxation behaviors.

Acknowledgements

This research was supported by the National Science Foundation of China (No. 11472164, 11332005 and 11072137), National Basic Research Program of China (2014CB046203), as well as & Shanghai Leading Academic Discipline Project (Grant No. S30106).

Notes and references

1 J. D. Ferry, *Viscoelastic properties of polymer*, Wiley, New York, 2nd edn, 1970.
2 J. E. Mark, *Physical properties of polymers handbook*, Springer, New York, 2007.
3 H. Hu, X. Zhang, Y. He, Z. S. Guo, J. Zhang and Y. Song, *J. Appl. Polym. Sci.*, 2013, **130**, 3161–3167.
4 Y. Zheng and G. McKenna, *Macromolecules*, 2003, **36**, 2387–2396.
5 D. Burnett, F. Thielmann and J. Booth, *Int. J. Pharm.*, 2004, **287**, 123–133.
6 L. C. E. Struik, *Physical aging in amorphous polymers and other materials*, Elsevier, Amsterdam, 1978.
7 A. Alegria, L. Goitiandia, I. Telleria and J. Colmenero, *Macromolecules*, 1997, **30**, 3881–3887.
8 A. R. Berens and I. Hodge, *Macromolecules*, 1982, **15**, 756–761.
9 C. Ho Huu and T. Vu-Khanh, *Theor. Appl. Fract. Mech.*, 2003, **40**, 75–83.
10 B. W. Rowe, B. D. Freeman and D. Paul, *Polymer*, 2010, **51**, 3784–3792.
11 B. W. Rowe, B. D. Freeman and D. R. Paul, *Macromolecules*, 2007, **40**, 2806–2813.
12 H. Sasabe and C. T. Moynihan, *J. Polym. Sci., Polym. Phys. Ed.*, 1978, **16**, 1447–1457.
13 S. Zervos, *Cellulose*, 2007, **14**, 375–384.
14 J. M. Hutchinson, *Prog. Polym. Sci.*, 1995, **20**, 703–760.
15 G. Odegard and A. Bandyopadhyay, *J. Polym. Sci., Part B: Polym. Phys.*, 2011, **49**, 1695–1716.
16 C. A. Angell, K. L. Ngai, G. B. McKenna, P. F. McMillan and S. W. Martin, *J. Appl. Phys.*, 2000, **88**, 3113–3157.
17 I. Hodge, *J. Non-Cryst. Solids*, 1994, **169**, 211–266.
18 D. Cangialosi, V. M. Boucher, A. Alegría and J. Colmenero, *Soft Matter*, 2013, **9**, 8619–8630.
19 D. Champion, C. Loupiac, D. Simatos, P. Lillford and P. Cayot, *Food Biophys.*, 2011, **6**, 160–169.
20 L. R. Bao, A. F. Yee and C. Y. C. Lee, *Polymer*, 2001, **42**, 7327–7333.
21 K. E. Secrist and A. J. Nolte, *Macromolecules*, 2011, **44**, 2859–2865.
22 S. Greco, J.-R. Authelin, C. Leveder and A. Segalini, *Pharm. Res.*, 2012, **29**, 2792–2805.
23 W. Knauss and V. Kenner, *J. Appl. Phys.*, 2008, **51**, 5131–5136.
24 M. Konidari, K. Papadokostaki and M. Sanopoulou, *J. Appl. Polym. Sci.*, 2011, **120**, 3381–3386.

25 K. Süvegh and R. Zelkó, *Macromolecules*, 2002, **35**, 795–800.
26 J. R. Martin and R. J. Gardner, *Polym. Eng. Sci.*, 1981, **21**, 557–565.
27 X. Shi, B. D. Fernando and S. G. Croll, *J. Coat. Technol. Res.*, 2008, **5**, 299–309.
28 C. Bockenheimer, D. Fata and W. Possart, *J. Appl. Polym. Sci.*, 2004, **91**, 369–377.
29 Y. Zheng, R. Priestley and G. McKenna, *J. Polym. Sci., Part B: Polym. Phys.*, 2004, **42**, 2107–2121.
30 G. B. McKenna, *J. Non-Cryst. Solids*, 2007, **353**, 3820–3828.
31 J. M. Cowie and R. Ferguson, *Polym. Commun.*, 1986, **27**, 258–260.
32 S. L. Maddox and J. K. Gillham, *J. Appl. Polym. Sci.*, 1997, **64**, 55–67.
33 J. K. Lee, J. Y. Hwang and J. Gillham, *J. Appl. Polym. Sci.*, 2001, **81**, 396–404.
34 H.-N. Lee and M. Ediger, *Macromolecules*, 2010, **43**, 5863–5873.
35 IGAsorp Moisture Sorption Analyser Manual, Hiden Analytical Ltd., 1997.
36 S. R. Aubuchon, *Am. Lab.*, 2009, **41**, 12–20.
37 R. Kohlrausch, *Poggendorff's Ann. Phys.*, 1954, **91**, 179–214.
38 G. Williams and D. C. Watts, *Trans. Faraday Soc.*, 1970, **66**, 80–85.
39 A. J. Kovacs, *Fortschr. Hochpolym.-Forsch.*, 1964, 394–507.
40 R. Bernstein and K. Gillen, *Polym. Degrad. Stab.*, 2010, **95**, 1471–1479.
41 J. F. Mano, *Macromol. Biosci.*, 2008, **8**, 69–76.
42 A. Lee and G. B. McKenna, *Polymer*, 1990, **31**, 423–430.
43 M. M. Santore, R. S. Duran and G. B. McKenna, *Polymer*, 1991, **32**, 2377–2381.
44 M. Alcoutlabi, F. Briatico-Vangosa and G. B. McKenna, *J. Polym. Sci., Part B: Polym. Phys.*, 2002, **40**, 2050–2064.
45 A. Flory and G. B. McKenna, *Mech. Time-Depend. Mater.*, 2010, **14**, 347–357.
46 X. Yuan, B. P. Carter and S. J. Schmidt, *J. Food Sci.*, 2011, **76**, E78–E89.
47 F. Doumenc, H. Bodiguel and B. Guerrier, *Eur. Phys. J. E: Soft Matter Biol. Phys.*, 2008, **27**, 3–11.
48 L. R. B. Louis and B. Rockland, *Water activity: theory and applications to food*, Marcel Dekker Inc, New York, 1987.
49 X. Yu, A. R. Schmidt, L. A. Bello-Perez and S. J. Schmidt, *J. Agric. Food Chem.*, 2007, **56**, 50–58.
50 L. C. Brinson and T. S. Gates, *Int. J. Solids Struct.*, 1995, **32**, 827–846.